bioRxiv preprint doi: https://doi.org/10.1101/2024.07.26.605237; this version posted July 26, 2024. The copyright holder for this preprint (which was not certified by peer review) is the author/funder, who has granted bioRxiv a license to display the preprint in perpetuity. It is made available under aCC-BY-NC-ND 4.0 International license.

1 # CD6 Regulates CD4 T Follicular Helper Cell Differentiation and Humoral
2 Immunity During Murine Coronavirus Infection
3
4 Running Title: CD6 Suppresses CD4 T Cell Activation
5
6 Amber Cardani-Boulton[1,2], Feng Lin[3,2], and Cornelia C Bergmann[1,2,#]
7
8
9 [1] Department of Neurosciences, Lerner Research Institute, Cleveland Clinic, Cleveland,
10 OH, USA
11 [2]Case Western Reserve University, Cleveland Clinic, Lerner College of Medicine
12 [3] Department of Immunity and Inflammation, Lerner Research Institute, Cleveland
13 Clinic, Cleveland, OH
14 [#]Address correspondence to Dr. Cornelia C. Bergmann, bergmac@ccf.org.
15

bioRxiv preprint doi: https://doi.org/10.1101/2024.07.26.605237; this version posted July 26, 2024. The copyright holder for this preprint (which was not certified by peer review) is the author/funder, who has granted bioRxiv a license to display the preprint in perpetuity. It is made available under aCC-BY-NC-ND 4.0 International license.

16 **Abstract (217 words)**

17 During activation the T cell transmembrane receptor CD6 becomes incorporated into
18 the T cell immunological synapse where it can exert both co-stimulatory and co-
19 inhibitory functions. Given the ability of CD6 to carry out opposing functions, this study
20 sought to determine how CD6 regulates early T cell activation in response to viral
21 infection. Infection of CD6 deficient mice with a neurotropic murine coronavirus resulted
22 in greater activation and expansion of CD4 T cells in the draining lymph nodes. Further
23 analysis demonstrated that there was also preferential differentiation of CD4 T cells into
24 T follicular helper cells, resulting in accelerated germinal center responses and
25 emergence of high affinity virus specific antibodies. Given that CD6 conversely supports
26 CD4 T cell activation in many autoimmune models, we probed potential mechanisms of
27 CD6 mediated suppression of CD4 T cell activation during viral infection. Analysis of
28 CD6 binding proteins revealed that infection induced upregulation of *Ubash3a,* a
29 negative regulator of T cell receptor signaling, was hindered in CD6 deficient lymph
30 nodes. Consistent with greater T cell activation and reduced UBASH3a activity, the T
31 cell receptor signal strength was intensified in CD6 deficient CD4 T cells. These results
32 reveal a novel immunoregulatory role for CD6 in limiting CD4 T cell activation and
33 deterring CD4 T follicular helper cell differentiation, thereby attenuating antiviral humoral
34 immunity.

35

36 **Importance (147 words)**

37 CD6 monoclonal blocking antibodies are being therapeutically administered to inhibit T
38 cell activation in autoimmune disorders. However, the multifaceted nature of CD6

bioRxiv preprint doi: https://doi.org/10.1101/2024.07.26.605237; this version posted July 26, 2024. The copyright holder for this preprint (which was not certified by peer review) is the author/funder, who has granted bioRxiv a license to display the preprint in perpetuity. It is made available under aCC-BY-NC-ND 4.0 International license.

39 allows for multiple and even opposing functions under different circumstances of T cell
40 activation. We therefore sought to characterize how CD6 regulates T cell activation in
41 the context viral infections using an *in vivo* murine coronavirus model. In contrast to its
42 role in autoimmunity, but consistent with its function in the presence of superantigens,
43 we found that CD6 deficiency enhances CD4 T cell activation and CD4 T cell help to
44 germinal center dependent antiviral humoral responses. Finally, we provide evidence
45 that CD6 regulates transcription of its intracellular binding partner UBASH3a, which
46 suppresses T cell receptor signaling and consequently T cell activation. These findings
47 highlight the context dependent flexibility of CD6 in regulating *in vivo* adaptive immune
48 responses, which may be targeted to enhance anti-viral immunity.

bioRxiv preprint doi: https://doi.org/10.1101/2024.07.26.605237; this version posted July 26, 2024. The copyright holder for this preprint (which was not certified by peer review) is the author/funder, who has granted bioRxiv a license to display the preprint in perpetuity. It is made available under aCC-BY-NC-ND 4.0 International license.

49 **Introduction**

50 T cell activation through engagement of the T cell receptor (TCR) is critical to
51 combat pathogens and tumors but can also cause detrimental injury if left unchecked.
52 For this reason, T cell activation is a highly complex process involving multiple layers of
53 regulation that are dependent on the concise orchestration of numerous signaling and
54 scaffolding proteins. Consequently, the diverse composition of the TCR signalosome
55 allows for significant flexibility in the strength of the TCR signal, which, rather than a
56 simple binary “yes or no” signal, the strength of the TCR governs T cell activation,
57 survival, and functional differentiation[1-4].

58 The intensity of the TCR signal is fine-tuned by, among other mechanisms, TCR
59 co-receptors that can enhance (co-stimulatory) or dampen (co-inhibitory) the TCR signal
60 strength. CD6 is a cell-surface glycoprotein that has been demonstrated to function as
61 both a TCR co-stimulatory or a co-inhibitory receptor during T cell activation in a context
62 dependent manner[5,6]. The functional heterogeneity of CD6 resides in its cytoplasmic
63 tail, which constitutes one of the longest leukocyte intracellular domains, thus making it
64 challenging to characterize the CD6 signaling cascade and identify mechanisms by
65 which it regulates TCR signaling [5-7]. A number of CD6 intracellular binding proteins that
66 positively propagate the TCR signal, most notably SLP76 and Zap70, have been
67 confirmed. Conversely, few CD6 signaling proteins that negatively regulate TCR
68 signaling have been identified. However, Ubiquitin associated and SH3 domain
69 containing A (UBASH3a), formally known as suppressor of T cell signaling 2 (STS-2),
70 was recently determined to directly interact with the cytoplasmic tail of CD6 [5-7].

bioRxiv preprint doi: https://doi.org/10.1101/2024.07.26.605237; this version posted July 26, 2024. The copyright holder for this preprint (which was not certified by peer review) is the author/funder, who has granted bioRxiv a license to display the preprint in perpetuity. It is made available under aCC-BY-NC-ND 4.0 International license.

71 While characterization of the CD6 signaling pathways remains incomplete, CD6
72 polymorphisms have been linked to either the susceptibility or severity of multiple
73 autoimmune diseases[9-11]. Furthermore, in preclinical murine models of autoimmunity,
74 inhibition of CD6 signaling was shown to prevent TCR co-stimulation, thereby limiting
75 activation of autoreactive T cells[15]. Therefore, monoclonal CD6 blocking antibodies
76 have been developed as clinical therapeutic treatments[8]. To this point, the anti-CD6
77 monoclonal antibody Itolizumab has been approved and is in use clinically in India for
78 the treatment of psoriasis[8]. CD6 blockade has also shown promise in clinical trials for
79 the treatment of rheumatoid arthritis and has recently gained interest as a potential
80 cancer therapy[12-14]. However, despite indications that CD6 has a suppressive role in
81 the presence of bacterial superantigens, the function of CD6 in the context of infectious
82 disease remains under-studied[16].
83 Given the opposing functions of CD6 in different disease and clinical settings, we
84 sought to determine how CD6 regulates T cell activation in an established model of viral
85 encephalomyelitis. The attenuated recombinant neurotropic murine beta coronavirus
86 MHV-A59 (mCoV), was chosen for this study as both the CD4 T helper 1 (TH1) cells
87 and cytotoxic CD8 T cells are essential for the control of infectious virus within the
88 CNS[17-20]. Furthermore, the generation of mCoV-specific antibodies is dependent on the
89 CD4 follicular helper (T_{FH}) cells, which mediate both germinal center (GC) formation as
90 well as somatic-hypermutation of the B cell immunoglobulin variable chain, thus
91 enabling the generation of high-affinity class switched antigen-specific B cells[20-22].
92 The study herein revealed that the absence of CD6 resulted in greater CD4 T cell
93 activation in the CNS draining cervical lymph nodes (cLNs) following mCoV infection.

bioRxiv preprint doi: https://doi.org/10.1101/2024.07.26.605237; this version posted July 26, 2024. The copyright holder for this preprint (which was not certified by peer review) is the author/funder, who has granted bioRxiv a license to display the preprint in perpetuity. It is made available under aCC-BY-NC-ND 4.0 International license.

94 An increase in total CD4 T cell numbers was accompanied by more pronounced
95 differentiation into CD4 T_{FH} cells. As a result, cLN GC reactions were accelerated,
96 complemented by the rapid appearance of high-affinity mCoV-specific antibodies in the
97 serum of CD6 knockout (KO) mice. Increased CD4 T cell activation in the absence of
98 CD6 was associated with impaired transcriptional upregulation of the established
99 negative regulator of TCR signaling *Ubash3a* [6-7]. In agreement with increased CD4 T
100 cell activation and decreased UBASH3a activity, the intensity of the TCR signal was
101 greater in CD6 deficient CD4 T cells. These data are the first to link CD6 with
102 transcriptional upregulation of *Ubash3a* and reveal pivotal novel roles of CD6 as a
103 negative regulator of antiviral CD4 T cell activation, CD4 T_{FH} cell differentiation, and
104 antiviral humoral responses. Overall, these results highlight the context dependent
105 functions of CD6 in regulating adaptive immune responses.

bioRxiv preprint doi: https://doi.org/10.1101/2024.07.26.605237; this version posted July 26, 2024. The copyright holder for this preprint (which was not certified by peer review) is the author/funder, who has granted bioRxiv a license to display the preprint in perpetuity. It is made available under aCC-BY-NC-ND 4.0 International license.

106 **Materials and Methods**

107 **Mice and Infections:** All procedures involving mice were approved by the Institutional
108 Animal Care and Use Committee of Cleveland Clinic and carried out in accordance with
109 the US Department of Health and Human Services Guide for the Care and Use of
110 Laboratory Animals and institutional guidelines. CD6 KO mice on the DBA-1
111 background were generated in the laboratory of Dr. Feng Lin and maintained under
112 pathogen-free conditions in the Cleveland Clinic Lerner Research Institute animal facility
113 [15]. WT controls were also maintained onsite and housed in the same room with
114 occasional supplementation as well as rejuvenation of the breeders with mice
115 purchased from Jackson Laboratory (strain number 000670). As previously reported[17,
116 21-23] 6–8-week-old gender matched male and female WT and CD6 KO mice were
117 intracranially (IC) infected with 10,000 PFU of the recombinant mCoV strain MHV-A59
118 whose non-essential open reading frame of gene 4 had been replaced with enhanced
119 green fluorescent protein and was generously provided by Dr. Das Sarma[24].

120

121 **Flow cytometry:** The CNS draining deep cLN, brains, and spinal cords were isolated
122 from phosphate buffer saline perfused mice. Tissues were finely minced, and single-
123 cell suspensions obtained after mechanical homogenization through a 70micron
124 strainer. Myelin was removed from CNS tissue by centrifugation at 850g for 45min at
125 4°C in 30% Percoll (Cytiva 17089101). After washing in 1X PBS, cells were
126 resuspended in FACS buffer (1X PBS, 1% BSA, +/- 0.1% NaN3) and stained with
127 fluorescently conjugated antibodies in the presence of FC block (clone 2.4G2) for 30min
128 at 4 degrees. The following antibodies were used: CD45 (clone 30-F11), CD3 (clone

bioRxiv preprint doi: https://doi.org/10.1101/2024.07.26.605237; this version posted July 26, 2024. The copyright holder for this preprint (which was not certified by peer review) is the author/funder, who has granted bioRxiv a license to display the preprint in perpetuity. It is made available under aCC-BY-NC-ND 4.0 International license.

129 17A2), CD4 (clone RM4-5), CD8 (clone 53-6.7), CD44 (clone IM7), CXCR5 (clone 2G8),
130 PD1 (clone 29F.1A12), CD6 (J90-462), CD19 clone (clone 1D3), IgD (clone 11-26c.2a),
131 GL7 (clone GL7), and CD138 (clone 281-2). After staining, cells were washed and
132 either resuspended in FACS buffer containing DAPI dye for immediate analysis or
133 stained with fixable live/dead dyes (Invitrogen Catalog number: L34957 or Beckman
134 Coulter Catalog number: C36628) according to manufacturer's protocol followed by
135 fixation in 4% PFA. The eBioscience FoxP3/ Transcription Factor Staining Kit was used
136 for intracellular staining according to the manufactures protocol. The following
137 antibodies were used: BCL6 (clone K112-91), Tbet (clone ebio4B10), and IRF4 (Clone
138 IRF.3E4) in the presence of FC block. Cells were collected using a 6-laser Beckman
139 CytoFLEX LX. The resulting data were compensated and analyzed with FlowJo
140 software (Tree Star, Inc., Ashland, OR) using the gating strategy exemplified in
141 Supplemental Figure 1.
142
143 **Immunofluorescence**: The CNS draining deep cLN were isolated from phosphate
144 buffer saline perfused mice and snap-frozen in Tissue-Tek O.C.T (Fisher). 10micron
145 slices were obtained using a Leica CM3050 cryostat and slide-mounted. Sections were
146 fixed in 4% PFA and permeabilized with Triton X-100. After blocking, cLNs were stained
147 with anti- CD3 (clone 17A2), GL7 (clone GL7), and B220 (clone RA3-6B2).
148 Corresponding secondary antibodies were used as necessary and sections were
149 mounted using ProLong Gold Antifade Mountant with DNA Stain DAPI. Entire cLNs
150 were scanned at 20X or 40X magnification using a Leica DM6B upright microscope

bioRxiv preprint doi: https://doi.org/10.1101/2024.07.26.605237; this version posted July 26, 2024. The copyright holder for this preprint (which was not certified by peer review) is the author/funder, who has granted bioRxiv a license to display the preprint in perpetuity. It is made available under aCC-BY-NC-ND 4.0 International license.

151 equipped for Fluorescence and Brightfield microscopy. Images were analyzed using
152 Image J software (NIH;
153 http://rsbweb.nih.gov/ij) implementing the FIJI plugin set (http://pacific.mpi-
154 cbg.de/wiki/index.php/Fiji).
155
156 **Quantitative real-time PCR:** The cLNs, brains, and spinal cords were isolated from
157 phosphate buffer saline perfused mice and immediately placed in trizol or Qiagen RLT
158 buffer on ice. Tissue was homogenized using the Qiagen TissueLyser with stainless-
159 steel beads and stored at -80°C. RNA was isolated according to the manufacturer's
160 instructions. Samples were DNaseI treated (Invitrogen Catalog number: 18068015)
161 according to the manufacturer's instructions and cDNA was synthesized using MMLV
162 reverse transcriptase (Invitrogen Catalog number: 28025021). Quantitative real-time
163 PCR was performed using PowerUp SYBR Green Master Mix (Fisher A25742) on a
164 7500 fast real-time PCR system (Applied Biosystems, Foster City, CA). Transcript levels
165 were calculated relative to the levels of the *Gapdh* housekeeping gene using the
166 following cycle threshold (C T) formula: 2 ^[CT(*Gapdh*) - CT(target gene)].
167 Primers for glyceraldehyde 3-phosphate dehydrogenase (*Gapdh*), activation-
168 induced cytidine deaminase (*Aicda*), T-box transcription factor 21 (*Tbx21*), and ubiquitin
169 associated and SH3 domain containing A (*UBASH3a*) were purchased for Sybr Green
170 analysis from Qiagen (Catalog number: 330001). All other primers are as follows:
171 *Il17* (F: CTCCACCGCAATGAAGAC and R: CTTTCCCTCCGCATTGAC),
172 *Foxp3* (F: CTGCTCCTCCTATTCCCGTAAC and R: AGCTAGAGGCTTTGCCTTCG),
173 *Ifng* (F: CCAAGTTTGAGGTCAACAACCC and R: AACAGCTGGTGGACCACTC),

bioRxiv preprint doi: https://doi.org/10.1101/2024.07.26.605237; this version posted July 26, 2024. The copyright holder for this preprint (which was not certified by peer review) is the author/funder, who has granted bioRxiv a license to display the preprint in perpetuity. It is made available under aCC-BY-NC-ND 4.0 International license.

174 mCoV-*N* (F: GCCAAATAATCGCGCTAGAA and R: CCGAGCTTAGCCAAAACAAG),
175 *Irf4* F: (GAACGAGGAGAAGAGCGTCTTC and R: GTAGGAGGATCTGGCTTGTCGA)
176

177 **mCoV-specific IgG ELISA and affinity index50:** As previously described[25-26], serum
178 collected from individual infected mice was serially diluted across virus-coated ELISA
179 plates. After incubation and washing, mCoV-specific antibodies bound to virus coated
180 plates were detected using HRP conjugated anti-mouse IgG antibodies, TMB substrate,
181 and ELISA stop solution. A dilution in which the fluorescence intensity was well within
182 the linear curve was used to determine differences between WT and CD6 KO mice
183 using optical density. Naïve controls were used to determine background signal. For
184 tissue antibody detection, whole tissue was placed in ice cold PBS and homogenized
185 using a Dounce Homogenizer. Cells and debris were removed by centrifugation and
186 the supernatant stored at -80º C prior to serial dilution as performed with serum
187 samples. Data was plotted across all dilutions tested.

188 At a concentration that was experimentally determined using the above mCoV-
189 specific ELISA, samples were incubated on virus-coated plates overnight. After
190 washing, serial dilutions of ammonium thiocyanate (3M-0M) were added to each sample
191 and incubated for 15min on a shaker at room temperature. After washing mCoV-
192 specific antibodies still bound to the virus coated plate were detected using HRP
193 conjugated anti-mouse IgG antibodies, TMB substrate, and ELISA stop solution. The
194 Affinity index 50 was determined as the concentration of ammonium thiocyanate at
195 which 50% of the antibody signal was lost[27-29].
196

bioRxiv preprint doi: https://doi.org/10.1101/2024.07.26.605237; this version posted July 26, 2024. The copyright holder for this preprint (which was not certified by peer review) is the author/funder, who has granted bioRxiv a license to display the preprint in perpetuity. It is made available under aCC-BY-NC-ND 4.0 International license.

197 **Statistics:** GraphPad Prism software was used to plot data points with SEM for error
198 bars. Statistical significance was determined using GraphPad Prism Software as
199 specified in the figure legends.

bioRxiv preprint doi: https://doi.org/10.1101/2024.07.26.605237; this version posted July 26, 2024. The copyright holder for this preprint (which was not certified by peer review) is the author/funder, who has granted bioRxiv a license to display the preprint in perpetuity. It is made available under aCC-BY-NC-ND 4.0 International license.

200 **Results**

201

202 **CD6 suppresses adaptive immune cell expansion and activation after mCoV**
203 **infection.**

204 To assess a potential role for CD6 in regulating T cell activation during viral
205 encephalomyelitis CD6 KO and wild type (WT) control mice were intracranially (IC)
206 infected with an attenuated recombinant murine Coronavirus (mCoV) strain MHV-A59[24].
207 In the absence of CD6 there was greater expansion of the CD4 T cells in the cLNs as
208 early as day 4 post infection (PI), which was sustained at day 7 PI (Figure 1A). In
209 addition, a greater percentage of CD4 T cells expressed high levels of the activation
210 marker CD44 (Figure 1B). Examination of the CD8 T cell population revealed
211 transiently increased expansion at day 4PI that contracted to WT levels by day 7 PI
212 (Figure 1C), although increased activation was evident at both days 4 and 7PI (Figure
213 1D). Importantly, no significant differences in T cell numbers or activation statuses were
214 observed in cLNs of naïve CD6 KO compared to WT mice (Figure 1A-D). Interestingly,
215 the total number of B cells in the CD6 KO cLNs was also elevated at day 7PI (Figure
216 1E). However, within the cLNs and brain CD6 was only detectable on CD4 and CD8 T
217 cells despite reports that CD6 is expressed on B1a B cells and some CD56 expressing
218 NK cells[30, 31] (Supplemental Figure 2A-D). Importantly, the increased lymphocyte
219 activation in the CD6 KO cLNs could not be attributed to increased viral loads as
220 transcripts of the mCoV nucleocapsid protein (N) were similar between WT and CD6
221 KO cLNs (Figure 1F). Therefore, inhibition of CD6 signaling resulted in greater CD4 T
222 cell activation and expansion, followed by increased B cell accumulation in the cLNs

bioRxiv preprint doi: https://doi.org/10.1101/2024.07.26.605237; this version posted July 26, 2024. The copyright holder for this preprint (which was not certified by peer review) is the author/funder, who has granted bioRxiv a license to display the preprint in perpetuity. It is made available under aCC-BY-NC-ND 4.0 International license.

223 after CNS infection with mCoV. These data contrasted studies of CD6 function in
224 experimental autoimmune models, but are consistent with *in vitro* analysis of CD6
225 during bacterial superantigen exposure[15-16, 46-47].
226

227 **CD6 regulates CD4 T helper cell differentiation.**

228 Given the expansion of cLN B cells, which do not express CD6, we next
229 examined if CD4 T_{FH} differentiation was altered in CD6 KO cLNs. Flow cytometry
230 analysis revealed that, even when normalized for the increase in total CD4 T cell
231 numbers, there was increased differentiation of CD4 T cells into T_{FH} cells (PD1^{+},
232 CXCR5^{+}) as early as day 4PI, which was sustained through at least day 7PI in CD6 KO
233 cLNs (Figure 2A). CD4 T cells expressing BCL6, the transcription factor essential for
234 T_{FH} cell differentiation, was also elevated in CD4 T cells from CD6 KO cLNs compared
235 to WT cLNs at day 4 and 7PI (Figure 2B)[32]. Conversely, the percent of CD4 T cells
236 expressing T-bet, the transcription factor essential for TH1 differentiation, was similar
237 between WT and CD6 KO mice[33] (Figure 2C). Therefore, the increase in total T-bet^{+}
238 CD4 T cells was consistent with the overall increase in total CD4 T cells and not greater
239 skewing towards TH1 differentiation. There was also no significant difference in *Ifng*
240 transcript levels indicating that the CD4 TH1 effector response was not significantly
241 altered in CD6 KO mice (Figure 2D). *Il17* mRNA could not be detected in either WT or
242 CD6 KO cLNs (data not shown), and no difference in *Foxp3* mRNA transcripts was
243 observed (Figure 2E). Taken together these data demonstrate that CD6 is able to limit
244 CD4 T_{FH} cell differentiation in addition to suppressing overall T cell activation and
245 expansion following mCoV infection.

bioRxiv preprint doi: https://doi.org/10.1101/2024.07.26.605237; this version posted July 26, 2024. The copyright holder for this preprint (which was not certified by peer review) is the author/funder, who has granted bioRxiv a license to display the preprint in perpetuity. It is made available under aCC-BY-NC-ND 4.0 International license.

246

247 **GC differentiation is enhanced in CD6 KOs during infection.**

248 To our knowledge this is the first time that CD6 has been linked to regulating T_{FH}
249 cell differentiation. We therefore analyzed the *in vivo* effector capacity of CD4 T_{FH} cells
250 generated in the CD6 KO mice by examining cLN GC formation. Subsequent to the
251 appearance of CD4 T_{FH} cells in the CD6 KO cLNs, a larger fraction of B cells in the CD6
252 KO cLNs had downregulated cell surface IgD, indicative of early activation (Figure 3A).
253 Similarly, a greater proportion of the already enlarged CD19 B cell population also
254 expressed the GC B cell marker GL7 at day 7 PI in CD6 KO cLNs (Figure 3B).
255 Accelerated GC reactions in CD6 KO cLNs were further confirmed by accelerated
256 transcription of *Aicda*, encoding the AID enzyme which is responsible for B cell somatic
257 hypermutation and antibody isotype switching[34] (Figure 3C). Therefore, accelerated and
258 enhanced CD4 T_{FH} cell differentiation was followed by increased B cell activation and
259 GC responses. We further confirmed that GC structures were properly forming within
260 CD6 KO cLNs at day 14PI, a time when GCs were easily discernable in WT cLNs, by
261 examining the accumulation of $GL7^+$ B cells within the cLN B cell follicle[20, 35, 36] (Figure
262 3D). Consistent with accelerated GC somatic hypermutation, mCoV-specific IgG
263 antibodies with increased affinity for mCoV were selectively detected in CD6 KO sera at
264 day 14PI (Figure 3E). Importantly, prior to GC formation we found no difference in the
265 affinity or concentrations of serum mCoV-specific IgG antibodies (Figure 3E-F).

266 Extended analysis of the GC responses revealed that cLN cellularity was
267 undergoing contraction by day 21 PI. However, contraction of the $CD45^+$ cellular
268 population was significantly greater in the CD6 KO cLNs (Supplemental Figure 3A).

bioRxiv preprint doi: https://doi.org/10.1101/2024.07.26.605237; this version posted July 26, 2024. The copyright holder for this preprint (which was not certified by peer review) is the author/funder, who has granted bioRxiv a license to display the preprint in perpetuity. It is made available under aCC-BY-NC-ND 4.0 International license.

269 Mirroring the CD45⁺ population, contraction of the CD4 T cell population was also
270 greater in CD6 KO mice at day 21PI (Supplemental Figure 3B). However, the
271 proportion of CD4 T_{FH} cells from the total CD4 T cell population was comparable
272 between CD6 KO and WT cLNs (Supplemental Figure 3C). B cell contraction was also
273 trended as increased in the CD6 KO cLNs at day 21PI, but did not reach statistical
274 significance (Supplemental Figure 3D). The relative proportion of $GL7^+$ GC B cells
275 within the IgD^- B cell population remained comparable between WT and CD6 KO cLNs
276 (Supplemental Figure 3E).
277 Analysis of the humoral response revealed that high-affinity serum mCoV-
278 specific IgG antibodies were detectable in WT mice by day 21 PI, but affinity was still
279 higher for mCoV-specific IgG antibodies in CD6 KO sera (Supplemental Figure 3F).
280 Intriguingly though, by day 28PI we could no longer detect significant differences in the
281 affinity of serum mCoV-specific IgG antibodies between WT and CD6 KO mice
282 (Supplemental Figure 3F). Semi-quantification of serum mCoV-specific IgG antibodies
283 also revealed that titers were transiently higher in the circulation of CD6 KO mice at day
284 21 but not at day 28 PI (Supplemental Figure 3F). Whether the enhanced contraction of
285 $CD45^+$ cells in CD6 KO cLNs is a direct result of an essential role for CD6 in sustaining
286 antiviral adaptive immune responses, or an indirect of some altered antiviral
287 pathogenesis in CD6 KO mice remains under investigation. Taken together these data
288 demonstrate that the increased CD4 T_{FH} cell differentiation in CD6 KO cLNs was
289 capable of driving accelerated B cell activation and functional GC responses leading to
290 accelerated secretion of high-affinity class-switched virus-specific antibodies.
291

bioRxiv preprint doi: https://doi.org/10.1101/2024.07.26.605237; this version posted July 26, 2024. The copyright holder for this preprint (which was not certified by peer review) is the author/funder, who has granted bioRxiv a license to display the preprint in perpetuity. It is made available under aCC-BY-NC-ND 4.0 International license.

292 **Expression of the CD6 intracellular binding protein UBASH3a is suppressed in**
293 **CD6 KO mice and coincides with stronger TCR signaling.**
294 To date, CD6 has predominantly function as a TCR co-stimulatory receptor
295 during T cell activation *in vitro*[6, 7, 37]. Therefore, characterization of the CD6 signaling
296 pathway has primarily identified positive regulators of TCR signaling[6, 7, 37]. However,
297 CD6 has also been shown to directly associate with the negative regulator of T cell
298 activation UBASH3a[6, 7]. Unexpectedly, *Ubash3a* transcription was substantially
299 upregulated in the cLNs of WT mice but was largely abrogated in CD6 KO cLNs in
300 response to mCoV infection (Figure 4A).
301 We therefore sought to substantiate a functional UBASH3a deficiency in CD6 KO
302 CD4 T cells *in vivo.* While the molecular functions of UBASH3a are poorly delineated, it
303 is established to have weak phosphatase activity[38, 39] and to negatively regulate cell-
304 surface TCR/CD3 complexes on CD4 T cells[40, 41]. In the absence of a defined mCoV-
305 epitope on the MHCII H-2^q background, and thus antigen-specific T cell tetramers, we
306 assessed CD3 expression on the entire CD44$^+$ CD4 T cell population, as well as early
307 differentiating CD4 T_{FH} cells. In the absence of CD6, cell-surface CD3 was modestly
308 increased in both total CD44$^+$ CD4 T cells (Figure 4B) and CD4 T_{FH} cells (Figure 4C).
309 While the degree of cell-surface CD3 elevation was minor, it was consistent with the
310 degree of change observed in UBASH3a knockdown studies[40]. These results supported
311 that CD6 may utilize UBASH3a to suppress T cell activation in cLNs during mCoV
312 infection.
313 As UBASH3a is a negative regulator of TCR signal strength, we next assessed
314 differences in the strength of TCR signal in cLN CD4 T cells from infected CD6 KO and

bioRxiv preprint doi: https://doi.org/10.1101/2024.07.26.605237; this version posted July 26, 2024. The copyright holder for this preprint (which was not certified by peer review) is the author/funder, who has granted bioRxiv a license to display the preprint in perpetuity. It is made available under aCC-BY-NC-ND 4.0 International license.

315 WT mice by measuring the transcription factor IRF4, an established dose-dependent
316 readout of the TCR signal strength[1, 4, 42-45]. Given the increase in GC responses *Irf4*
317 transcripts were unsurprisingly highly elevated by day 7 PI in CD6 KO compared to WT
318 cLNs (Figure 4D). Target analysis of CD4 T cell populations by flow cytometry
319 confirmed that a higher percentage of CD6 KO CD44$^+$ CD4 T cells express high levels
320 of IRF4, signifying that CD6 KO T cells had stronger TCR signaling after mCoV infection
321 (Figure 4E). During the early stages of CD4 T_{FH} cell differentiation (day 4PI), CD6 KO
322 CD4 T_{FH} cells also displayed elevated IRF4 expression (Figure 4F-G). However, by day
323 7PI all of the CD4 T_{FH} cells were IRF4 positive, with most being IRF4^{high} (Figure 4F).
324 Taken together, these data strongly implicate that CD6 suppresses T cell activation
325 during mCoV infection through UBASH3a mediated negative regulation of the TCR
326 signaling.
327
328 **CD6 regulates peripheral, but not CNS, humoral immunity during mCoV induced**
329 **encephalomyelitis.**
330 We next examined the adaptive immune responses within the mCoV infected
331 CNS. Consistent with greater activation and expansion in the cLN, CD4 T cell numbers
332 were elevated in the CD6 KO infected brain at day 7PI (Figure 5A). On the other hand,
333 CD8 T cell infiltration of the brain was not significantly altered at day 7PI (Figure 5B).
334 *Ifng* transcripts were similar between WT and CD6 KO brains (Figure 5C) and *Il17*
335 transcripts remained undetectable (Figure 5D). The elevated total number of CD4 T
336 cells in CD6 KO infected brains was thus not associated with overt differences in T cell
337 effector activity. Furthermore, comparable antiviral effector T cell responses were

bioRxiv preprint doi: https://doi.org/10.1101/2024.07.26.605237; this version posted July 26, 2024. The copyright holder for this preprint (which was not certified by peer review) is the author/funder, who has granted bioRxiv a license to display the preprint in perpetuity. It is made available under aCC-BY-NC-ND 4.0 International license.

338 supported by congruent kinetics of viral control between WT and CD6 KO brains and
339 spinal cords as measured by viral nucleocapsid (N) specific transcripts (Figure 5E).
340 The total number of B cells in the CD6 KO mCoV infected brains was also
341 elevated at day 7PI (Figure 5F). This was notable as most of the B cells in the brain at
342 this early timepoint are $IgD^{+}IgM^{+}$ B cells that migrate to the CNS in response to the
343 inflammation[20-21]. More surprisingly, analysis of supernatants from dissociated WT and
344 CD6 KO brain and spinal cord tissue revealed similar levels of virus-specific IgG
345 antibodies across multiple dilutions as well as comparable mCoV affinity at day 21PI
346 (Figure 5G-H). Therefore, while CD6 KO mice transiently had greater mCoV-specific
347 IgG responses in the periphery at day 21PI (Supplemental Figure 3 F), there were no
348 detectable changes within the infected CNS at this time point. Thus, these data
349 implicated that CD6 predominantly regulates the peripheral CD4 T cell and humoral
350 responses at the priming site, with minimal impact in the infected CNS during mCoV
351 infection.
352

bioRxiv preprint doi: https://doi.org/10.1101/2024.07.26.605237; this version posted July 26, 2024. The copyright holder for this preprint (which was not certified by peer review) is the author/funder, who has granted bioRxiv a license to display the preprint in perpetuity. It is made available under aCC-BY-NC-ND 4.0 International license.

353 **Discussion**

354 The dual functions of CD6 as a positive and negative regulator of T cell activation
355 are well established, but its influence on T cell responses during viral infections have
356 not been studied. In this report, we investigated how the absence of CD6 affects T cell
357 activation using a neurotropic mCoV model, in which CD4 and CD8 T cells are both
358 essential to control infectious virus. Our results demonstrate that CD6 acts as a
359 negative regulator of CD4 T cell activation in CNS draining cLN following virus infection.
360 In addition, we have discovered a previously unrecognized role for CD6 in limiting
361 CD4T_{FH} cell differentiation and, by extension, delaying GC responses. These novel
362 findings have significant clinical implications for patients receiving therapeutic CD6
363 blocking antibody treatments.

364 The function of CD6 as a negative regulator of T cell activation during mCoV
365 encephalomyelitis stands in stark contrast to its co-stimulatory role in multiple
366 autoimmune models including autoimmune encephalitis and autoimmune uveitis [5-6, 15-16,
367 46-47]. Importantly, the opposing functions of CD6 in CD4 T cell activation are not easily
368 attributed to murine intrinsic factors, as the CD6 KO mice used herein were generated
369 from the same colony and housed in the same facility as in the above mentioned
370 autoimmune studies[15-16]. Unfortunately, further comparison between autoimmune and
371 virus models is complicated by numerous factors; In the autoimmune encephalomyelitis
372 and uveitis models T cell activation is dependent on immunization with self-peptide or
373 antigen in adjuvant resulting in the induction of both Th1 and Th17 CD4 T cells[15, 46],
374 whereas virus-specific T cells are activated by replicating virus and presentation of viral
375 antigen generating an exclusive Th1 response[17-20]. These models also utilize distinct

bioRxiv preprint doi: https://doi.org/10.1101/2024.07.26.605237; this version posted July 26, 2024. The copyright holder for this preprint (which was not certified by peer review) is the author/funder, who has granted bioRxiv a license to display the preprint in perpetuity. It is made available under aCC-BY-NC-ND 4.0 International license.

376 innate immune scavenging, pattern recognition receptors, and antigen presenting cells,
377 all of which also contribute to the outcome of T cell activation[48-50]. It is thus reasonable
378 that such distinct innate input signals *in viv*o would influence differential expression of
379 the extracellular CD6 ligands and/ or CD6 intracellular interacting proteins, leading to
380 distinct outcomes of CD6 signaling.

381 To this end, analysis of the established CD6 intracellular signaling proteins
382 identified UBASH3A as a primary candidate responsible for CD6 mediated dampening
383 of CD4 T cell activation following mCoV infection. *Ubash3a* mRNA transcripts increased
384 in the cLNs of WT mice, while upregulation was drastically impaired in CD6 KO cLNS.
385 Consistent with UBASH3a knockdown studies and diminished UBASH3a activity, cLN
386 CD4 T cells from CD6 KO mice had modest, but significantly, increased accumulation of
387 cell-surface CD3[40]. While these fairly minor changes in increased cell-surface CD3/TCR
388 complexes are unlikely to result in enhanced T cell activation, as few as 500 TCR
389 complexes have been implicated to be sufficient for T cell activation *in vivo*[51].
390 UBASH3a is incompletely characterized, but is known to suppress TCR signaling, at
391 least in part through suppression of ZAP-70 signaling in a ubiquitin and phosphatase-
392 dependent manner[39, 52-53]. Since TCR signaling is established to directly upregulate
393 IRF4 in a dose-dependent manner in both CD8 and CD4 T cells[43, 44, 45], IRF4 expression
394 was used as a readout to measure how loss of UBASH3a in CD6 KO mice affected the
395 TCR signal strength. Indeed, IRF4 protein levels were higher in CD6 KO CD4T cells
396 compared to WT CD4 T cells from the cLNs, confirming that the absence of CD6
397 produced a stronger TCR signal. Overall, the novel finding that CD6 influences
398 *Ubash3a* expression in the mCoV infection model implicates that UBASH3a exerts

bioRxiv preprint doi: https://doi.org/10.1101/2024.07.26.605237; this version posted July 26, 2024. The copyright holder for this preprint (which was not certified by peer review) is the author/funder, who has granted bioRxiv a license to display the preprint in perpetuity. It is made available under aCC-BY-NC-ND 4.0 International license.

399 inhibitory effects on TCR signaling through CD6. Although UBASH3a is known to
400 suppress T cell activation and proliferation *in vitro* and in autoimmune diabetes[54],
401 UBASH3a regulation has not been explored in studies focusing on CD6. Therefore,
402 analysis of UBASH3a in autoimmune diseases where CD6 acts as a positive regulator
403 of T cell activation may shed light on the pathogenic role of CD6.

404 Unexpectedly, CD6 KO CD4 T cells also showed preferential differentiation into
405 CD4 T_{FH} effectors. While TCR-signal strength is an established determinate of T helper
406 cell differentiation[1-4], mechanistic studies to assess how CD6 signaling proteins,
407 including UBASH3a, regulate CD4 T_{FH} cell differentiation will require the development of
408 complex *in vitro* assays that mimic T cell activation during mCoV infection *in vivo*.
409 Nevertheless, the accelerated and enhanced T_{FH} cell development correlated with
410 earlier and elevated titers of high-affinity class-switched virus-specific antibodies in the
411 serum of CD6 KO mice. Of note, the difference in the total number of $CD44^+$ CD4 T
412 cells could not be completely explained by the magnitude of change in CD4 T_{FH} cells.
413 As we were unable to detect changes in other CD4 T helper cells, and there are
414 indications that both CD6 KO and UBASH3a KO T cells may have a lower threshold for
415 activation homeostatically, it is likely that there is some degree of non-specific T cell
416 recruitment and activation contributing to the greater accumulation of CD4 T cell in the
417 CD6 KO cLNs[15, 60].

418 Distinct from the periphery, we found no difference in mCoV-specific IgG
419 antibodies within the CNS itself. We are currently investigating whether early changes
420 in the CD6 KO cLNs alters the differentiation, survival, or migratory capacity acquired of
421 antibody secreting cells during GC differentiation[55]. To this end, it is worth noting that

bioRxiv preprint doi: https://doi.org/10.1101/2024.07.26.605237; this version posted July 26, 2024. The copyright holder for this preprint (which was not certified by peer review) is the author/funder, who has granted bioRxiv a license to display the preprint in perpetuity. It is made available under aCC-BY-NC-ND 4.0 International license.

422 the predominant ligand of CD6, CD166, was found to be essential for pathogenic B cells
423 to infiltrate the CNS during experimental autoimmune encephalitis[56]. Interestingly
424 though, while CD6 appears to facilitate T cell migration in autoimmune
425 encephalomyelitis[15], it was redundant for T cell infiltration into the virally infected CNS.
426 This redundancy may also explain why CD6 was essential to sustain dendritic cell-T cell
427 interaction during antigen presentation *in vitro*, but not in this *in vivo* setting[61].

428 Overall, these data indicate that the clinically used CD6 blocking antibody
429 treatments may be beneficial to antiviral immunity. A limitation of the mCoV model is
430 that acute viral replication in the CNS is controlled by T cells and not the humoral
431 response, which was reflected in the similar kinetics of virus control between the WT
432 and CD6 KO CNS. Therefore, the biological significance of the accelerated antiviral-
433 humoral response in the absence of CD6 may be more readily revealed in a model
434 where GC-derived humoral responses are essential to prevent viral dissemination to the
435 CNS. CD6 may also potentially be exploited during the administration of traditional and
436 mRNA-based vaccines. As Itolizumab has been in use in India since 2013 and given
437 the number of clinical trials ongoing during the COIVD-19 pandemic, it may be feasible
438 to examine antiviral humoral responses during vaccination as well as primary SARS-
439 CoV2 infections in patients that had been receiving CD6 monoclonal blocking antibody
440 therapies[8, 12, 57-59].

441 In summary, we have identified novel roles for CD6 as a negative regulator of
442 both CD4 T cell and GC-derived antiviral humoral responses. CD6 inhibition of these
443 responses appears to be T cell intrinsic and associated with a deficit in UBASH3a
444 mediated suppression of CD4 T cell TCR signal. The number of ongoing clinical trials

bioRxiv preprint doi: https://doi.org/10.1101/2024.07.26.605237; this version posted July 26, 2024. The copyright holder for this preprint (which was not certified by peer review) is the author/funder, who has granted bioRxiv a license to display the preprint in perpetuity. It is made available under aCC-BY-NC-ND 4.0 International license.

445 examining the efficacy of CD6 blockade necessitates further interrogation of its role
446 during viral infections and vaccination, especially given the context dependent role of
447 CD6 in T cell activation.
448

bioRxiv preprint doi: https://doi.org/10.1101/2024.07.26.605237; this version posted July 26, 2024. The copyright holder for this preprint (which was not certified by peer review) is the author/funder, who has granted bioRxiv a license to display the preprint in perpetuity. It is made available under aCC-BY-NC-ND 4.0 International license.

449 Acknowledgements

450 This work was supported by the Nation Institute of Health R01 NS086299 (C.B.) and

451 R01 EY034077 (F.L)

452

453 **Author Contributions**

454 A.C-B. and C.C.B. Study conception and design; A.C-B. Acquired and Analyzed data;

455 A.C-B. wrote the manuscript; C.C.B. and F.L. Edited the manuscript; F.L and C.C.B.,

456 Providing funding/ reagents and supervision.

457

458 **Competing Interests**

459 A.C-B and C.C.B declare no competing interests. F.L. is founder and CSO of Abcon,

460 which focuses on CD6-ADC in the treatment of T cell lymphoma. Abcon was not

461 involved with this manuscript, including experimental design, data acquisition and

462 interpretation.

463

bioRxiv preprint doi: https://doi.org/10.1101/2024.07.26.605237; this version posted July 26, 2024. The copyright holder for this preprint (which was not certified by peer review) is the author/funder, who has granted bioRxiv a license to display the preprint in perpetuity. It is made available under aCC-BY-NC-ND 4.0 International license.

464 **References**
465

466 1. Tubo NJ, Jenkins MK. TCR signal quantity and quality in CD4⁺ T cell
467 differentiation. Trends Immunol. 2014 Dec;35(12):591-596. doi:
468 10.1016/j.it.2014.09.008. Epub 2014 Oct 22. PMID: 25457838; PMCID:
469 PMC4406772.
470
471 2. Künzli M, Reuther P, Pinschewer DD, King CG. Opposing effects of T cell
472 receptor signal strength on CD4 T cells responding to acute versus chronic viral
473 infection. Elife. 2021 Mar 8;10:e61869. doi: 10.7554/eLife.61869. PMID:
474 33684030; PMCID: PMC7943189.
475
476 3. Snook JP, Kim C, Williams MA. TCR signal strength controls the differentiation of
477 CD4⁺ effector and memory T cells. Sci Immunol. 2018 Jul 20;3(25):eaas9103.
478 doi: 10.1126/sciimmunol.aas9103. PMID: 30030369; PMCID: PMC6126666.
479
480 4. Bhattacharyya ND, Feng CG. Regulation of T Helper Cell Fate by TCR Signal
481 Strength. Front Immunol. 2020 May 19;11:624. doi: 10.3389/fimmu.2020.00624.
482 PMID: 32508803; PMCID: PMC7248325.
483
484 5. Gonçalves CM, Henriques SN, Santos RF, Carmo AM. CD6, a Rheostat-Type
485 Signalosome That Tunes T Cell Activation. Front Immunol. 2018 Dec 18;9:2994.
486 doi: 10.3389/fimmu.2018.02994. PMID: 30619347; PMCID: PMC6305463.
487
488 6. Mori D, Grégoire C, Voisinne G, Celis-Gutierrez J, Aussel R, Girard L, Camus M,
489 Marcellin M, Argenty J, Burlet-Schiltz O, Fiore F, Gonzalez de Peredo A,
490 Malissen M, Roncagalli R, Malissen B. The T cell CD6 receptor operates a
491 multitask signalosome with opposite functions in T cell activation. J Exp Med.
492 2021 Feb 1;218(2):e20201011. doi: 10.1084/jem.20201011. PMID: 33125054;
493 PMCID: PMC7608068.
494
495 7. Voisinne G, Locard-Paulet M, Froment C, Maturin E, Menoita MG, Girard L,
496 Mellado V, Burlet-Schiltz O, Malissen B, Gonzalez de Peredo A, Roncagalli R.
497 Kinetic proofreading through the multi-step activation of the ZAP70 kinase
498 underlies early T cell ligand discrimination. Nat Immunol. 2022 Sep;23(9):1355-
499 1364. doi: 10.1038/s41590-022-01288-x. Epub 2022 Aug 31. PMID: 36045187;
500 PMCID: PMC9477740.
501
502 8. Krupashankar DS, Dogra S, Kura M, Saraswat A, Budamakuntla L, Sumathy TK,
503 Shah R, Gopal MG, Narayana Rao T, Srinivas CR, Bhat R, Shetty N, Manmohan
504 G, Sai Krishna K, Padmaja D, Pratap DV, Garg V, Gupta S, Pandey N, Khopkar
505 U, Montero E, Ramakrishnan MS, Nair P, Ganapathi PC. Efficacy and safety of
506 itolizumab, a novel anti-CD6 monoclonal antibody, in patients with moderate to
507 severe chronic plaque psoriasis: results of a double-blind, randomized, placebo-
508 controlled, phase-III study. J Am Acad Dermatol. 2014 Sep;71(3):484-92. doi:
509 10.1016/j.jaad.2014.01.897. Epub 2014 Apr 2. PMID: 24703722.

bioRxiv preprint doi: https://doi.org/10.1101/2024.07.26.605237; this version posted July 26, 2024. The copyright holder for this preprint (which was not certified by peer review) is the author/funder, who has granted bioRxiv a license to display the preprint in perpetuity. It is made available under aCC-BY-NC-ND 4.0 International license.

510
511 9. De Jager PL, Jia X, Wang J, de Bakker PI, Ottoboni L, Aggarwal NT, Piccio L,
512 Raychaudhuri S, Tran D, Aubin C, Briskin R, Romano S; International MS
513 Genetics Consortium; Baranzini SE, McCauley JL, Pericak-Vance MA, Haines
514 JL, Gibson RA, Naeglin Y, Uitdehaag B, Matthews PM, Kappos L, Polman C,
515 McArdle WL, Strachan DP, Evans D, Cross AH, Daly MJ, Compston A, Sawcer
516 SJ, Weiner HL, Hauser SL, Hafler DA, Oksenberg JR. Meta-analysis of genome
517 scans and replication identify CD6, IRF8 and TNFRSF1A as new multiple
518 sclerosis susceptibility loci. Nat Genet. 2009 Jul;41(7):776-82. doi:
519 10.1038/ng.401. Epub 2009 Jun 14. PMID: 19525953; PMCID: PMC2757648.
520
521 10. Zheng M, Zhang L, Yu H, Hu J, Cao Q, Huang G, Huang Y, Yuan G, Kijlstra A,
522 Yang P. Genetic polymorphisms of cell adhesion molecules in Behcet's disease
523 in a Chinese Han population. Sci Rep. 2016 Apr 25;6:24974. doi:
524 10.1038/srep24974. PMID: 27108704; PMCID: PMC4842956.
525
526 11. Consuegra-Fernández M, Julià M, Martínez-Florensa M, Aranda F, Català C,
527 Armiger-Borràs N, Arias MT, Santiago F, Guilabert A, Esteve A, Muñoz C,
528 Ferrándiz C, Carrascosa JM, Pedrosa E, Romaní J, Alsina M, Mascaró-Galy JM,
529 Lozano F. Genetic and experimental evidence for the involvement of the CD6
530 lymphocyte receptor in psoriasis. Cell Mol Immunol. 2018 Oct;15(10):898-906.
531 doi: 10.1038/cmi.2017.119. Epub 2017 Dec 11. PMID: 29225340; PMCID:
532 PMC6207571.
533
534 12. Rodríguez PC, Prada DM, Moreno E, Aira LE, Molinero C, López AM, Gómez
535 JA, Hernández IM, Martínez JP, Reyes Y, Milera JM, Hernández MV, Torres R,
536 Avila Y, Barrese Y, Viada C, Montero E, Hernández P. The anti-CD6 antibody
537 itolizumab provides clinical benefit without lymphopenia in rheumatoid arthritis
538 patients: results from a 6-month, open-label Phase I clinical trial. Clin Exp
539 Immunol. 2018 Feb;191(2):229-239. doi: 10.1111/cei.13061. Epub 2017 Nov 16.
540 PMID: 28963724; PMCID: PMC5758380.
541
542 13. Ruth JH, Gurrea-Rubio M, Athukorala KS, Rasmussen SM, Weber DP, Randon
543 PM, Gedert RJ, Lind ME, Amin MA, Campbell PL, Tsou PS, Mao-Draayer Y, Wu
544 Q, Lanigan TM, Keshamouni VG, Singer NG, Lin F, Fox DA. CD6 is a target for
545 cancer immunotherapy. JCI Insight. 2021 Mar 8;6(5):e145662. doi:
546 10.1172/jci.insight.145662. PMID: 33497367; PMCID: PMC8021120.
547
548 14. Gurrea-Rubio M, Wu Q, Amin MA, Tsou PS, Campbell PL, Amarista CI, Ikari Y,
549 Brodie WD, Mattichak MN, Muraoka S, Randon PM, Lind ME, Ruth JH, Mao-
550 Draayer Y, Ding S, Shen X, Cooney LA, Lin F, Fox DA. Activation of cytotoxic
551 lymphocytes through CD6 enhances killing of cancer cells. Cancer Immunol
552 Immunother. 2024 Jan 27;73(2):34. doi: 10.1007/s00262-023-03578-1. PMID:
553 38280067; PMCID: PMC10821976.
554

bioRxiv preprint doi: https://doi.org/10.1101/2024.07.26.605237; this version posted July 26, 2024. The copyright holder for this preprint (which was not certified by peer review) is the author/funder, who has granted bioRxiv a license to display the preprint in perpetuity. It is made available under aCC-BY-NC-ND 4.0 International license.

555 15. Li Y, Singer NG, Whitbred J, Bowen MA, Fox DA, Lin F. CD6 as a potential target
556 for treating multiple sclerosis. Proc Natl Acad Sci U S A. 2017 Mar
557 7;114(10):2687-2692. doi: 10.1073/pnas.1615253114. Epub 2017 Feb 16. PMID:
558 28209777; PMCID: PMC5347585.
559
560 16. Henriques, S.N., Oliveira, L., Santos, R.F. *et al.* CD6-mediated inhibition of T cell
561 activation via modulation of Ras. *Cell Commun Signal* **20**, 184 (2022).
562 https://doi.org/10.1186/s12964-022-00998-x
563
564 17. Cowley TJ, Weiss SR. Murine coronavirus neuropathogenesis: determinants of
565 virulence. J Neurovirol. 2010 Nov;16(6):427-34. doi:
566 10.3109/13550284.2010.529238. Epub 2010 Nov 12. PMID: 21073281; PMCID:
567 PMC3153983.
568
569 18. Stohlman SA, Bergmann CC, Lin MT, Cua DJ, Hinton DR (1998). CTL effector
570 function within the central nervous system requires CD4+ T cells. J Immunol 160:
571 2896–2904.
572
573 19. Sussman MA, Shubin RA, Kyuwa S, Stohlman SA (1989). T-cell-mediated
574 clearance of mouse hepatitis virus strain JHM from the central nervous system. J
575 Virol 63: 3051–3061.
576
577 20. Cardani-Boulton A, Boylan BT, Stetsenko V, Bergmann CC. B cells going viral in
578 the CNS: Dynamics, complexities, and functions of B cells responding to viral
579 encephalitis. Immunol Rev. 2022 Oct;311(1):75-89. doi: 10.1111/imr.13124.
580 Epub 2022 Aug 19. PMID: 35984298; PMCID: PMC9804320.
581
582 21. Atkinson JR, Bergmann CC. Protective Humoral Immunity in the Central Nervous
583 System Requires Peripheral CD19-Dependent Germinal Center Formation
584 following Coronavirus Encephalomyelitis. J Virol. 2017 Nov 14;91(23):e01352-17.
585 doi: 10.1128/JVI.01352-17. PMID: 28931676; PMCID: PMC5686739.
586
587 22. Lin MT, Hinton DR, Marten NW, Bergmann CC, Stohlman SA (1999). Antibody
588 prevents virus reactivation within the central nervous system. J Immunol
589 162:7358–7368.
590
591 23. Matthews AE, Weiss SR, Shlomchik MJ, Hannum LG, Gombold JL, Paterson Y.
592 Antibody is required for clearance of infectious murine hepatitis virus A59 from
593 the central nervous system, but not the liver. J Immunol. 2001 Nov
594 1;167(9):5254-63. doi: 10.4049/jimmunol.167.9.5254. PMID: 11673540.
595
596 24. Das Sarma J, Scheen E, Seo SH, Koval M, Weiss SR. Enhanced green
597 fluorescent protein expression may be used to monitor murine coronavirus
598 spread in vitro and in the mouse central nervous system. J Neurovirol. 2002
599 Oct;8(5):381-91. doi: 10.1080/13550280260422686. PMID: 12402164; PMCID:
600 PMC7095158.

bioRxiv preprint doi: https://doi.org/10.1101/2024.07.26.605237; this version posted July 26, 2024. The copyright holder for this preprint (which was not certified by peer review) is the author/funder, who has granted bioRxiv a license to display the preprint in perpetuity. It is made available under aCC-BY-NC-ND 4.0 International license.

601
602
603 25. Akache B, Stark FC, McCluskie MJ. Measurement of Antigen-Specific IgG Titers
604 by Direct ELISA. Methods Mol Biol. 2021;2183:537-547. doi: 10.1007/978-1-
605 0716-0795-4_31. PMID: 32959266.
606
607 26. Amber Cardani-Boulton, Sun-Sang J. Sung, William A. Petri, Young S. Hahn,
608 Thomas J. Braciale; Leptin Receptor Deficiency Impairs Lymph Node
609 Development and Adaptive Immune Response. J Immunol 2024; ji2100985.
610 https://doi.org/10.4049/jimmunol.2100985
611
612 27. Metcalf TU, Griffin DE. Alphavirus-induced encephalomyelitis: antibody-secreting
613 cells and viral clearance from the nervous system. J Virol. 2011
614 Nov;85(21):11490-501. doi: 10.1128/JVI.05379-11. Epub 2011 Aug 24. PMID:
615 21865385; PMCID: PMC3194963.
616
617 28. Pullen GR, Fitzgerald MG, Hosking CS. Antibody avidity determination by ELISA
618 using thiocyanate elution. J Immunol Methods. 1986 Jan 22;86(1):83-7. doi:
619 10.1016/0022-1759(86)90268-1. PMID: 3944471.
620
621 29. Macdonald RA, Hosking CS, Jones CL. The measurement of relative antibody
622 affinity by ELISA using thiocyanate elution. J Immunol Methods. 1988 Feb
623 10;106(2):191-4. doi: 10.1016/0022-1759(88)90196-2. PMID: 3339255.
624
625 30. Enyindah-Asonye G, Li Y, Xin W, Singer NG, Gupta N, Fung J, Lin F. CD6
626 Receptor Regulates Intestinal Ischemia/Reperfusion-induced Injury by
627 Modulating Natural IgM-producing B1a Cell Self-renewal. J Biol Chem. 2017 Jan
628 13;292(2):661-671. doi: 10.1074/jbc.M116.749804. Epub 2016 Dec 1. PMID:
629 27909060; PMCID: PMC5241740.
630
631 31. Braun M, Müller B, ter Meer D, Raffegerst S, Simm B, Wilde S, Spranger S,
632 Ellwart J, Mosetter B, Umansky L, Lerchl T, Schendel DJ, Falk CS. The CD6
633 scavenger receptor is differentially expressed on a CD56 natural killer cell
634 subpopulation and contributes to natural killer-derived cytokine and chemokine
635 secretion. J Innate Immun. 2011;3(4):420-34. doi: 10.1159/000322720. Epub
636 2010 Dec 18. PMID: 21178331.
637
638 32. Choi J, Crotty S. Bcl6-Mediated Transcriptional Regulation of Follicular Helper T
639 cells (TFH). Trends Immunol. 2021 Apr;42(4):336-349. doi:
640 10.1016/j.it.2021.02.002. Epub 2021 Mar 1. PMID: 33663954; PMCID:
641 PMC8021443.
642
643 33. Szabo SJ, Kim ST, Costa GL, Zhang X, Fathman CG, Glimcher LH. A novel
644 transcription factor, T-bet, directs Th1 lineage commitment. Cell. 2000 Mar
645 17;100(6):655-69. doi: 10.1016/s0092-8674(00)80702-3. PMID: 10761931.
646

bioRxiv preprint doi: https://doi.org/10.1101/2024.07.26.605237; this version posted July 26, 2024. The copyright holder for this preprint (which was not certified by peer review) is the author/funder, who has granted bioRxiv a license to display the preprint in perpetuity. It is made available under aCC-BY-NC-ND 4.0 International license.

647 34. Okazaki IM, Kinoshita K, Muramatsu M, Yoshikawa K, Honjo T. The AID enzyme
648 induces class switch recombination in fibroblasts. Nature. 2002 Mar
649 21;416(6878):340-5. doi: 10.1038/nature727. Epub 2002 Mar 3. PMID:
650 11875397.
651
652 35. Cyster JG, Allen CDC. B Cell Responses: Cell Interaction Dynamics and
653 Decisions. Cell. 2019 Apr 18;177(3):524-540. doi: 10.1016/j.cell.2019.03.016.
654 PMID: 31002794; PMCID: PMC6538279.
655
656 36. Laidlaw BJ, Cyster JG. Transcriptional regulation of memory B cell differentiation.
657 Nat Rev Immunol. 2021 Apr;21(4):209-220. doi: 10.1038/s41577-020-00446-2.
658 Epub 2020 Oct 6. PMID: 33024284; PMCID: PMC7538181.
659
660 37. Roncagalli R, Hauri S, Fiore F, Liang Y, Chen Z, Sansoni A, Kanduri K, Joly R,
661 Malzac A, Lähdesmäki H, Lahesmaa R, Yamasaki S, Saito T, Malissen M,
662 Aebersold R, Gstaiger M, Malissen B. Quantitative proteomics analysis of
663 signalosome dynamics in primary T cells identifies the surface receptor CD6 as a
664 Lat adaptor-independent TCR signaling hub. Nat Immunol. 2014 Apr;15(4):384-
665 392. doi: 10.1038/ni.2843. Epub 2014 Mar 2. PMID: 24584089; PMCID:
666 PMC4037560.
667
668 38. Mikhailik A, Ford B, Keller J, Chen Y, Nassar N, Carpino N. A phosphatase
669 activity of Sts-1 contributes to the suppression of TCR signaling. Mol Cell. 2007
670 Aug 3;27(3):486-97. doi: 10.1016/j.molcel.2007.06.015. PMID: 17679096;
671 PMCID: PMC2709417.
672
673 39. Luis BS, Carpino N. Insights into the suppressor of T-cell receptor (TCR)
674 signaling-1 (Sts-1)-mediated regulation of TCR signaling through the use of novel
675 substrate-trapping Sts-1 phosphatase variants. FEBS J. 2014 Feb;281(3):696-
676 707. doi: 10.1111/febs.12615. Epub 2013 Dec 12. PMID: 24256567; PMCID:
677 PMC3968691.
678
679 40. Ge Y, Paisie TK, Chen S, Concannon P. UBASH3A Regulates the Synthesis and
680 Dynamics of TCR-CD3 Complexes. J Immunol. 2019 Dec 1;203(11):2827-2836.
681 doi: 10.4049/jimmunol.1801338. Epub 2019 Oct 28. PMID: 31659016; PMCID:
682 PMC6938261.
683
684 41. Voisinne G, García-Blesa A, Chaoui K, Fiore F, Bergot E, Girard L, Malissen M,
685 Burlet-Schiltz O, Gonzalez de Peredo A, Malissen B, Roncagalli R. Co-
686 recruitment analysis of the CBL and CBLB signalosomes in primary T cells
687 identifies CD5 as a key regulator of TCR-induced ubiquitylation. Mol Syst Biol.
688 2016 Jul 29;12(7):876. doi: 10.15252/msb.20166837. PMID: 27474268; PMCID:
689 PMC4965873.
690
691 42. Yao S, Buzo BF, Pham D, Jiang L, Taparowsky EJ, Kaplan MH, Sun J. Interferon
692 regulatory factor 4 sustains CD8(+) T cell expansion and effector differentiation.

bioRxiv preprint doi: https://doi.org/10.1101/2024.07.26.605237; this version posted July 26, 2024. The copyright holder for this preprint (which was not certified by peer review) is the author/funder, who has granted bioRxiv a license to display the preprint in perpetuity. It is made available under aCC-BY-NC-ND 4.0 International license.

693 Immunity. 2013 Nov 14;39(5):833-45. doi: 10.1016/j.immuni.2013.10.007. Epub
694 2013 Nov 7. PMID: 24211184; PMCID: PMC3855863.
695
696 43. Wu H, Witzl A, Ueno H. Assessment of TCR signal strength of antigen-specific
697 memory CD8+ T cells in human blood. Blood Adv. 2019 Jul 23;3(14):2153-2163.
698 doi: 10.1182/bloodadvances.2019000292. PMID: 31320320; PMCID:
699 PMC6650739.
700
701 44. Allison KA, Sajti E, Collier JG, Gosselin D, Troutman TD, Stone EL, Hedrick SM,
702 Glass CK. Affinity and dose of TCR engagement yield proportional enhancer and
703 gene activity in CD4+ T cells. Elife. 2016 Jul 4;5:e10134. doi:
704 10.7554/eLife.10134. PMID: 27376549; PMCID: PMC4931909.
705
706 45. Man K, Miasari M, Shi W, Xin A, Henstridge DC, Preston S, Pellegrini M, Belz
707 GT, Smyth GK, Febbraio MA, Nutt SL, Kallies A. The transcription factor IRF4 is
708 essential for TCR affinity-mediated metabolic programming and clonal expansion
709 of T cells. Nat Immunol. 2013 Nov;14(11):1155-65. doi: 10.1038/ni.2710. Epub
710 2013 Sep 22. Erratum in: Nat Immunol. 2014 Sep;15(9):894. PMID: 24056747.
711
712 46. Zhang L, Li Y, Qiu W, Bell BA, Dvorina N, Baldwin WM 3rd, Singer N, Kern T,
713 Caspi RR, Fox DA, Lin F. Targeting CD6 for the treatment of experimental
714 autoimmune uveitis. J Autoimmun. 2018 Jun;90:84-93. doi:
715 10.1016/j.jaut.2018.02.004. Epub 2018 Feb 19. PMID: 29472120; PMCID:
716 PMC5949263
717
718 47. Li Y, Ruth JH, Rasmussen SM, Athukorala KS, Weber DP, Amin MA, Campbell
719 PL, Singer NG, Fox DA, Lin F. Attenuation of Murine Collagen-Induced Arthritis
720 by Targeting CD6. Arthritis Rheumatol. 2020 Sep;72(9):1505-1513. doi:
721 10.1002/art.41288. Epub 2020 Aug 14. PMID: 32307907; PMCID: PMC7745675.
722
723 48. Marta M, Meier UC, Lobell A. Regulation of autoimmune encephalomyelitis by
724 toll-like receptors. Autoimmun Rev. 2009 May;8(6):506-9. doi:
725 10.1016/j.autrev.2009.01.006. Epub 2009 Jan 27. PMID: 19211042.
726
727 49. Zalinger ZB, Elliott R, Rose KM, Weiss SR. MDA5 Is Critical to Host Defense
728 during Infection with Murine Coronavirus. J Virol. 2015 Dec;89(24):12330-40. doi:
729 10.1128/JVI.01470-15. Epub 2015 Sep 30. PMID: 26423942; PMCID:
730 PMC4665247.
731
732 50. Diebold M, Fehrenbacher L, Frosch M, Prinz M. How myeloid cells shape
733 experimental autoimmune encephalomyelitis: At the crossroads of outside-in
734 immunity. Eur J Immunol. 2023 Oct;53(10):e2250234. doi:
735 10.1002/eji.202250234. Epub 2023 Aug 21. PMID: 37505465.
736

bioRxiv preprint doi: https://doi.org/10.1101/2024.07.26.605237; this version posted July 26, 2024. The copyright holder for this preprint (which was not certified by peer review) is the author/funder, who has granted bioRxiv a license to display the preprint in perpetuity. It is made available under aCC-BY-NC-ND 4.0 International license.

737
738 51. Labrecque N, Whitfield LS, Obst R, Waltzinger C, Benoist C, Mathis D. How
739 much TCR does a T cell need? Immunity. 2001 Jul;15(1):71-82. doi:
740 10.1016/s1074-7613(01)00170-4. PMID: 11485739.
741
742 52. Yang M, Chen T, Li X, Yu Z, Tang S, Wang C, Gu Y, Liu Y, Xu S, Li W, Zhang X,
743 Wang J, Cao X. K33-linked polyubiquitination of Zap70 by Nrdp1 controls CD8(+)
744 T cell activation. Nat Immunol. 2015 Dec;16(12):1253-62. doi: 10.1038/ni.3258.
745 Epub 2015 Sep 21. Erratum in: Nat Immunol. 2020 Mar;21(3):355. PMID:
746 26390156.
747
748 53. Carpino N, Chen Y, Nassar N, Oh HW. The Sts proteins target tyrosine
749 phosphorylated, ubiquitinated proteins within TCR signaling pathways. Mol
750 Immunol. 2009 Oct;46(16):3224-31. doi: 10.1016/j.molimm.2009.08.015. Epub
751 2009 Sep 5. PMID: 19733910; PMCID: PMC2757469.
752
753 54. Chen YG, Ciecko AE, Khaja S, Grzybowski M, Geurts AM, Lieberman SM.
754 UBASH3A deficiency accelerates type 1 diabetes development and enhances
755 salivary gland inflammation in NOD mice. Sci Rep. 2020 Jul 21;10(1):12019. doi:
756 10.1038/s41598-020-68956-6. PMID: 32694640; PMCID: PMC7374577.
757
758 55. Marques CP, Kapil P, Hinton DR, Hindinger C, Nutt SL, Ransohoff RM, Phares
759 TW, Stohlman SA, Bergmann CC. CXCR3-dependent plasma blast migration to
760 the central nervous system during viral encephalomyelitis. J Virol. 2011
761 Jul;85(13):6136-47. doi: 10.1128/JVI.00202-11. Epub 2011 Apr 20. PMID:
762 21507985; PMCID: PMC3126522.
763
764 56. Michel L, Grasmuck C, Charabati M, Lécuyer MA, Zandee S, Dhaeze T, Alvarez
765 JI, Li R, Larouche S, Bourbonnière L, Moumdjian R, Bouthillier A, Lahav B,
766 Duquette P, Bar-Or A, Gommerman JL, Peelen E, Prat A. Activated leukocyte
767 cell adhesion molecule regulates B lymphocyte migration across central nervous
768 system barriers. Sci Transl Med. 2019 Nov 13;11(518):eaaw0475. doi:
769 10.1126/scitranslmed.aaw0475. PMID: 31723036.
770
771 57. Caballero A, Filgueira LM, Betancourt J, Sánchez N, Hidalgo C, Ramírez A,
772 Martinez A, Despaigne RE, Escalona A, Diaz H, Meriño E, Ortega LM, Castillo U,
773 Ramos M, Saavedra D, García Y, Lorenzo G, Cepeda M, Arencibia M, Cabrera
774 L, Domecq M, Estévez D, Valenzuela C, Lorenzo P, Sánchez L, Mazorra Z, León
775 K, Crombet T. Treatment of COVID-19 patients with the anti-CD6 antibody
776 itolizumab. Clin Transl Immunology. 2020 Nov 25;9(11):e1218. doi:
777 10.1002/cti2.1218. PMID: 33304584; PMCID: PMC7688906.
778
779 58. Díaz Y, Ramos-Suzarte M, Martín Y, Calderón NA, Santiago W, Viñet O, La O Y,
780 Oyarzábal JPA, Pérez Y, Lorenzo G, Cepeda M, Saavedra D, Mazorra Z,
781 Estevez D, Lorenzo-Luaces P, Valenzuela C, Caballero A, Leon K, Crombet T,
782 Hidalgo CJ. Use of a Humanized Anti-CD6 Monoclonal Antibody (Itolizumab) in

bioRxiv preprint doi: https://doi.org/10.1101/2024.07.26.605237; this version posted July 26, 2024. The copyright holder for this preprint (which was not certified by peer review) is the author/funder, who has granted bioRxiv a license to display the preprint in perpetuity. It is made available under aCC-BY-NC-ND 4.0 International license.

783 Elderly Patients with Moderate COVID-19. Gerontology. 2020;66(6):553-561. doi:
784 10.1159/000512210. Epub 2020 Oct 26. PMID: 33105142; PMCID:
785 PMC7649683
786
787 59. Saavedra D, Añé-Kourí AL, Sánchez N, Filgueira LM, Betancourt J, Herrera C,
788 Manso L, Chávez E, Caballero A, Hidalgo C, Lorenzo G, Cepeda M, Valenzuela
789 C, Ramos M, León K, Mazorra Z, Crombet T. An anti-CD6 monoclonal antibody
790 (itolizumab) reduces circulating IL-6 in severe COVID-19 elderly patients. Immun
791 Ageing. 2020 Nov 14;17(1):34. doi: 10.1186/s12979-020-00207-8. PMID:
792 33292350; PMCID: PMC7666403.
793
794 60. Castro-Sánchez P, Aguilar-Sopeña O, Alegre-Gómez S, Ramirez-Munoz R,
795 Roda-Navarro P. Regulation of $CD4^+$ T Cell Signaling and Immunological
796 Synapse by Protein Tyrosine Phosphatases: Molecular Mechanisms in
797 Autoimmunity. Front Immunol. 2019 Jun 26;10:1447. doi:
798 10.3389/fimmu.2019.01447. PMID: 31297117; PMCID: PMC6607956.
799
800 61. Zimmerman AW, Joosten B, Torensma R, Parnes JR, van Leeuwen FN, Figdor
801 CG. Long-term engagement of CD6 and ALCAM is essential for T-cell
802 proliferation induced by dendritic cells. Blood. 2006 Apr 15;107(8):3212-20. doi:
803 10.1182/blood-2005-09-3881. Epub 2005 Dec 13. PMID: 16352806.
804

bioRxiv preprint doi: https://doi.org/10.1101/2024.07.26.605237; this version posted July 26, 2024. The copyright holder for this preprint (which was not certified by peer review) is the author/funder, who has granted bioRxiv a license to display the preprint in perpetuity. It is made available under aCC-BY-NC-ND 4.0 International license.

805 **Figure 1: CD6 deficiency results in enhanced adaptive immune cell expansion**
806 **and activation in the cervical lymph nodes after mCoV infection.** cLNs from WT
807 and CD6 KO mice infected with 10,000 PFU of mCoV were taken at the indicated
808 time points and analyzed by flow cytometry for the A) total number of CD4 T cells, B)
809 percent of CD4 T cells that are CD44 high, C) total number of CD8 T cells, D)
810 percent of CD8 T cells that are CD44 high, and E) total number of CD19 B cells.
811 cLNs were also analyzed by F) qRT-PCR for transcripts of the mCoV nucleocapsid
812 gene (N). Each data point represents a single mouse and a minimum of two
813 individual experiments were pooled for each time point. Significance was
814 determined using a Two-way ANOVA with a Bonferroni's post-hoc test and denoted
815 as * for $p<0.05$, ** for $p<0.01$, *** for $p<0.001$, and **** for $p<0.0001$.
816

bioRxiv preprint doi: https://doi.org/10.1101/2024.07.26.605237; this version posted July 26, 2024. The copyright holder for this preprint (which was not certified by peer review) is the author/funder, who has granted bioRxiv a license to display the preprint in perpetuity. It is made available under aCC-BY-NC-ND 4.0 International license.

817 **Figure 2: CD6 regulates CD4 T helper cell differentiation in cervical lymph**
818 **nodes after mCoV infection.** cLNs from mCoV infected WT and CD6 KO mice
819 were taken at the indicated time points and analyzed by flow cytometry for the
820 proportion and number of CD4 T cells that are **A)** T_{FH} cells (CXCR5$^+$, PD1$^+$), **B)**
821 BCL6$^+$, and **C)** T-Bet$^+$. cLNs s were also analyzed by qRT-PCR for **D)** *Ifng* and **E)**
822 *Foxp3* transcripts. Each data point represents a single mouse with experiments
823 pooled from a minimum of two independent experiments for each time point. Flow
824 cytometry plots and histograms are of a representative WT(black) and CD6 KO (red)
825 mouse. FMO staining controls (gray) were included in the day 4PI histograms.
826 Significance was determined using a Two-way ANOVA with a Bonferroni's post-hoc
827 test or an unpaired T-test and denoted as * for p<0.05, ** for p<0.01, *** for
828 p<0.001,and **** for p<0.0001.
829

bioRxiv preprint doi: https://doi.org/10.1101/2024.07.26.605237; this version posted July 26, 2024. The copyright holder for this preprint (which was not certified by peer review) is the author/funder, who has granted bioRxiv a license to display the preprint in perpetuity. It is made available under aCC-BY-NC-ND 4.0 International license.

830 **Figure 3: Germinal centers are enhanced in the absence of CD6.** WT and CD6
831 KO mice were infected with mCoV. At day 4 and 7PI cLN CD19$^+$ B cells were
832 examined by flow cytometry for expression of **A)** IgD or **B)** GL7 (denoting germinal
833 center B cells). Additionally, qRT-PCR was used to analyze expression of **C)** *Aicda*
834 in cLNs. Day 14PI flash fozen cLNs were **D**) stained for B220 (red), GL7 (green),
835 and CD3 (blue) to confirm GC formation within B cell zones. Serum collected at days
836 4, 7, and 14 PI was analyzed for mCoV-specific IgG **E)** avidity index$_{50}$ and **F)** titers
837 by ELISA. "()" indicates the experimentally determined concentration of the serum
838 dilution used for the analysis. Each data point represents a single mouse and a
839 minimum of two experiments were pooled for each time point. Flow plots are of a
840 representative mouse. Significance was determined by Two-way ANOVA using a
841 Bonferroni's post-hoc test and denoted as * for p<0.05, ** for p<0.01, *** for
842 p<0.001,and **** for p<0.0001.
843

bioRxiv preprint doi: https://doi.org/10.1101/2024.07.26.605237; this version posted July 26, 2024. The copyright holder for this preprint (which was not certified by peer review) is the author/funder, who has granted bioRxiv a license to display the preprint in perpetuity. It is made available under aCC-BY-NC-ND 4.0 International license.

844 **Figure 4: CD6-mediated control of *Ubahs3a* expression corresponds with**
845 **decreased TCR signal strength.** cLNs from mCoV infected WT and CD6 KO mice
846 were isolated at the indicated time points. **A)** *Ubash3a* expression was quantified by
847 qRT-PCR. The MFI of CD3 on **B)** $CD44^+$ CD4 T cells and **C)** CD4 T_{FH} cells at day
848 4PI was used to monitor cell-surface CD3/TCR by flow cytometry. **D)** *Irf4*
849 transcription in the cLNs was quantified by qRT-PCR. The percent of **E)** CD44+
850 CD4 T cells and **F)** CD4 T_{FH} cells that are $IRF4^{high}$ in the cLN as well as the **G)** MFI
851 of IRF4 on CD44+ CD4 T_{FH} cells was analyzed by flow cytometry. Each data point
852 represents a single mouse and representative histograms are of one WT mouse in
853 grey and one CD6 KO mouse in red. **B, C,** and **H** are data representative of a
854 minimum of 2 experiments. Significance was determined by Two-way ANOVA using
855 a Bonferroni's post-hoc test (A, D, E) or by unpaired T-Test (B-C and F-G) and
856 denoted as * for p<0.05, ** for p<0.01, *** for p<0.001,and **** for p<0.0001.
857

bioRxiv preprint doi: https://doi.org/10.1101/2024.07.26.605237; this version posted July 26, 2024. The copyright holder for this preprint (which was not certified by peer review) is the author/funder, who has granted bioRxiv a license to display the preprint in perpetuity. It is made available under aCC-BY-NC-ND 4.0 International license.

858 **Figure 5: CD6 regulates peripheral, but not CNS, immune responses.** CNS
859 tissues were isolated from WT and CD6 KO mice at the indicated time points. The
860 total number of **A)** CD4 T cells and **B)** CD8 T cells were quantified by flow
861 cytometry. mRNA transcripts of **C)** *Ifng,* **D)** *Il17,* and **E)** viral *N* gene were quantified
862 in the indicated CNS tissues. The total number of **F)** CD19 B cells in the brain was
863 quantified by flow cytometry. mCoV-specific IgG antibodies in the CNS tissues were
864 **G)** semi-quantified and **H)** measured for affinity using an avidity $index_{50}$ assay. Each
865 data point represents a single mouse. Significance was determined by A-B) Two-
866 way ANOVA using a Bonferroni's post-hoc test, C-D) unpaired T-Test and E-G)
867 Two-way ANOVA using a Bonferroni's post-hoc test and denoted as * for p<0.05, **
868 for p<0.01, *** for p<0.001,and **** for p<0.0001.
869

bioRxiv preprint doi: https://doi.org/10.1101/2024.07.26.605237; this version posted July 26, 2024. The copyright holder for this preprint (which was not certified by peer review) is the author/funder, who has granted bioRxiv a license to display the preprint in perpetuity. It is made available under aCC-BY-NC-ND 4.0 International license.

870 **Supplemental Figure 1: Representative gating strategy of mCoV infected cLNs**
871 **at day 7PI. S**inglet cells that fell into a lymphocyte FSC, SSC gate were analyzed for
872 cell viability using a live/dead dye. CD45+ live cells were then first A) analyzed for
873 CD3e expression followed by CD4 or CD8 expression. CD4 expressing T cells were
874 then analyzed for activation CD44 and T_{FH} cells by CXCR5 and PD1 co-expression.
875 B) CD45+ cells were also analyzed for CD19, followed by GL7 expression or IgD
876 expression. Finally, IgD- B cells were examined for CD138.
877

bioRxiv preprint doi: https://doi.org/10.1101/2024.07.26.605237; this version posted July 26, 2024. The copyright holder for this preprint (which was not certified by peer review) is the author/funder, who has granted bioRxiv a license to display the preprint in perpetuity. It is made available under aCC-BY-NC-ND 4.0 International license.

878 **Supplemental Figure 2: CD6 is expressed on CD4 and CD8 T cells.** A) cLNs
879 and B) brains from naïve WT (n=4) and CD6 KO (n=2) mice were analyzed by flow
880 cytometry for CD6 expression on the indicated population. Representative
881 histograms of CD6 expression in the naïve cLNs are shown in the left panel of (A).
882 C) Representative flow cytometry plots from the naïve cLNs (left) and brain (right)
883 demonstrating no detectable CD6 expression on $CD45^{-}$ cells. D) Representative
884 histograms of cLNs were taken at day 4 (left) and 7 (right) PI of CD6 expression on
885 live cells with T cells gated out. E) CD6 expression on activated T cells at day 4PI in
886 the cLNs was confirmed by flow cytometry. All cells were identified by flow
887 cytometery using the gating scheme depicted in Supplemental Figure 1. Each data
888 point represents an individual mouse and representative histograms and flow plots
889 are from an individual WT (red) and CD6 KO (grey) mouse.
890

bioRxiv preprint doi: https://doi.org/10.1101/2024.07.26.605237; this version posted July 26, 2024. The copyright holder for this preprint (which was not certified by peer review) is the author/funder, who has granted bioRxiv a license to display the preprint in perpetuity. It is made available under aCC-BY-NC-ND 4.0 International license.

891 **Supplemental Figure 3: Contraction in the cLNs is accelerated in CD6 KO**
892 **mice.** cLNs from WT and CD6 KO mice were analyzed by flow cytometry at the
893 indicated time point(s) to quantify **A)** total $CD45^+$ cells (simplified graph of day 21PI
894 alone on the right to illustrate the difference in contraction), **B)** total CD4 T cells **C)**
895 the fraction of CD4 T cells that are CD4 T_{FH} cells, **D)** total CD19 cells, and **E)** the
896 percent of IgD^- B cells that are GC B cells. At days 21 and 28 PI the mCoV-specific
897 IgG antibody **F)** avidity $index_{50}$ (left) and titers (right) were measured across multiple
898 experiments. For all graphs each data points represents an individual mouse.
899 Significance was determined by Two-way ANOVA using a Bonferroni's post-hoc test
900 or an unpaired T test and denoted as * for p<0.05, ** for p<0.01, *** for p<0.001,and
901 **** for p<0.0001.

bioRxiv preprint doi: https://doi.org/10.1101/2024.07.26.605237; this version posted July 26, 2024. The copyright holder for this preprint (which was not certified by peer review) is the author/funder, who has granted bioRxiv a license to display the preprint in perpetuity. It is made available under aCC-BY-NC-ND 4.0 International license.

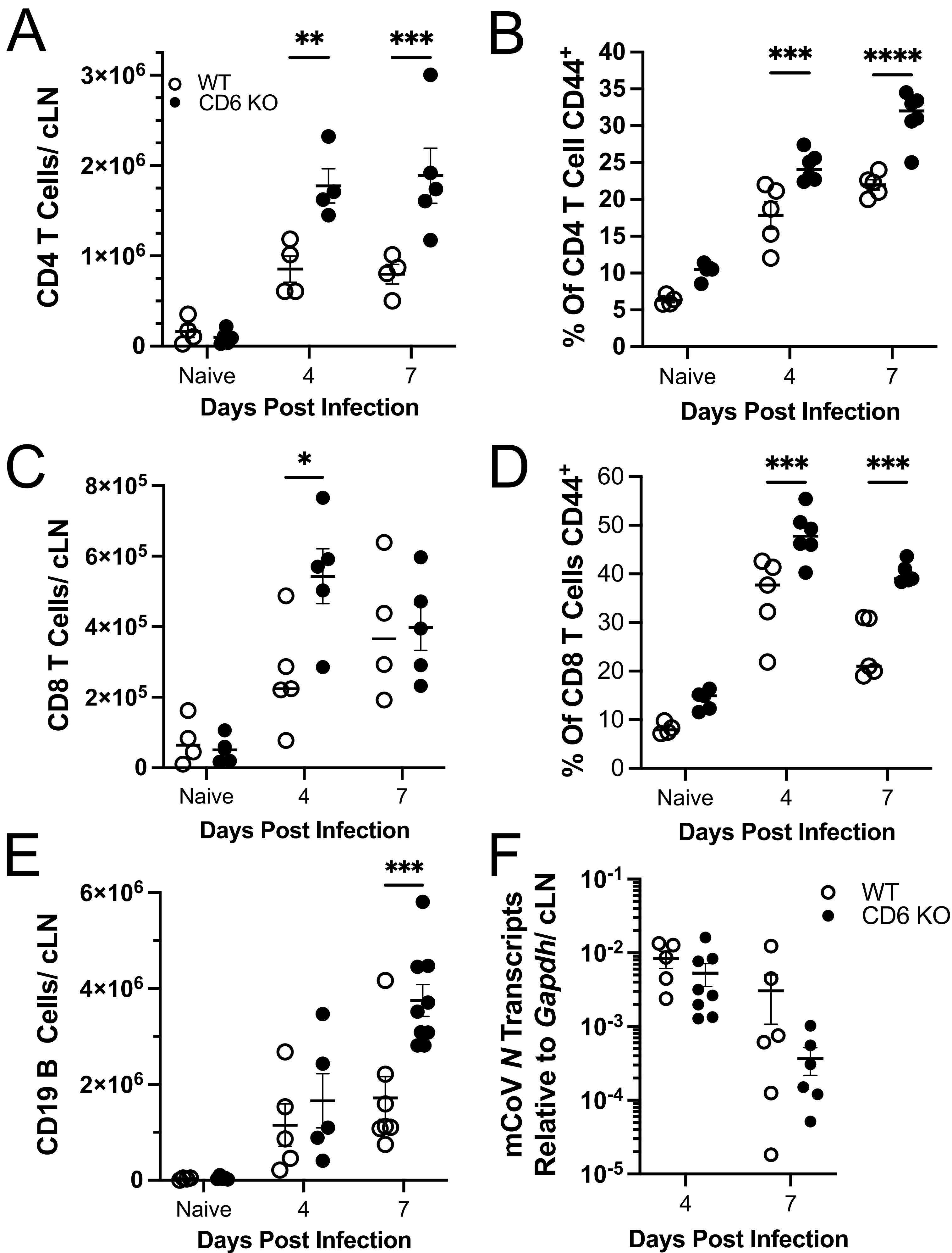

bioRxiv preprint doi: https://doi.org/10.1101/2024.07.26.605237; this version posted July 26, 2024. The copyright holder for this preprint (which was not certified by peer review) is the author/funder, who has granted bioRxiv a license to display the preprint in perpetuity. It is made available under aCC-BY-NC-ND 4.0 International license.

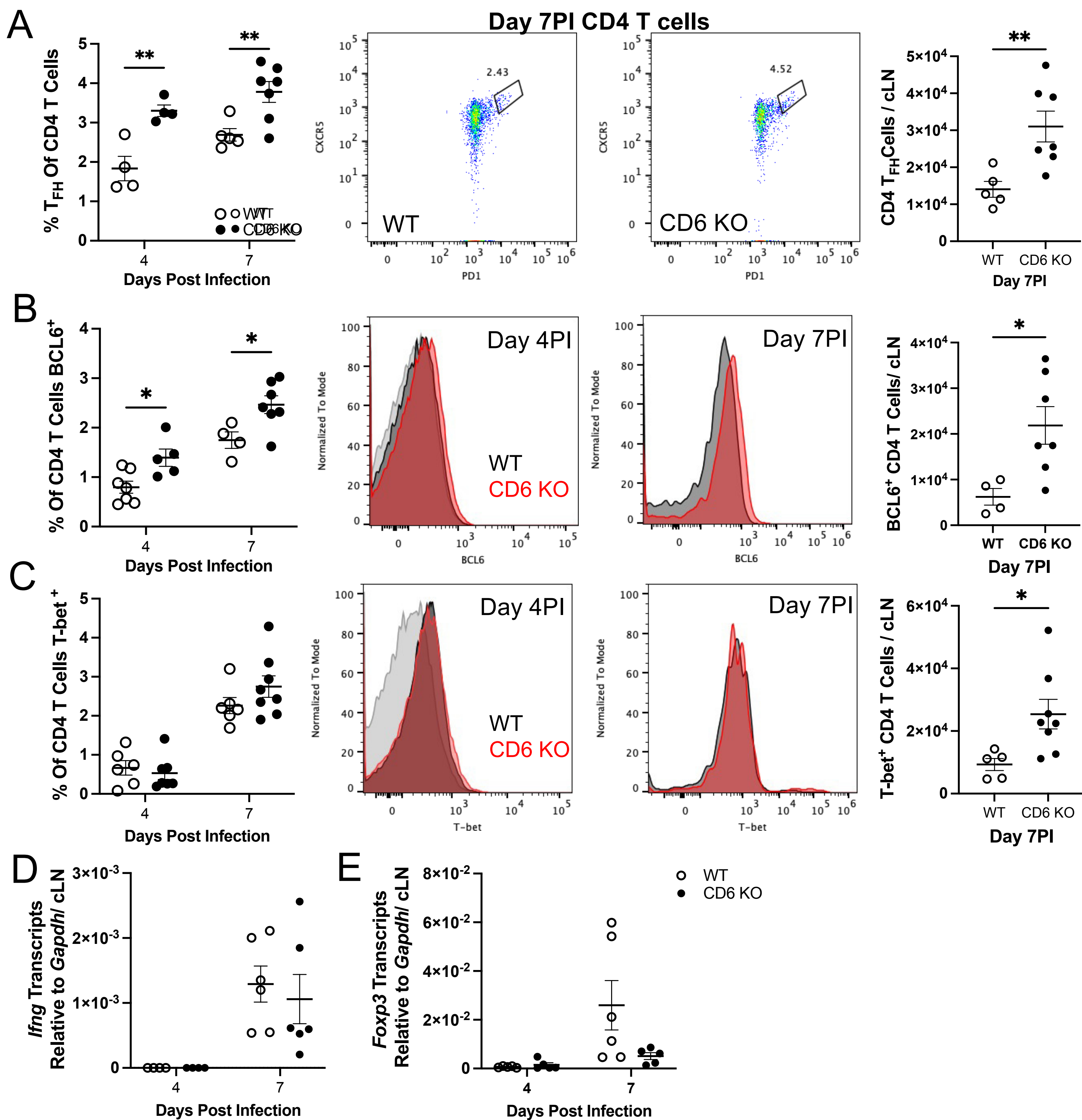

bioRxiv preprint doi: https://doi.org/10.1101/2024.07.26.605237; this version posted July 26, 2024. The copyright holder for this preprint (which was not certified by peer review) is the author/funder, who has granted bioRxiv a license to display the preprint in perpetuity. It is made available under aCC-BY-NC-ND 4.0 International license.

bioRxiv preprint doi: https://doi.org/10.1101/2024.07.26.605237; this version posted July 26, 2024. The copyright holder for this preprint (which was not certified by peer review) is the author/funder, who has granted bioRxiv a license to display the preprint in perpetuity. It is made available under aCC-BY-NC-ND 4.0 International license.

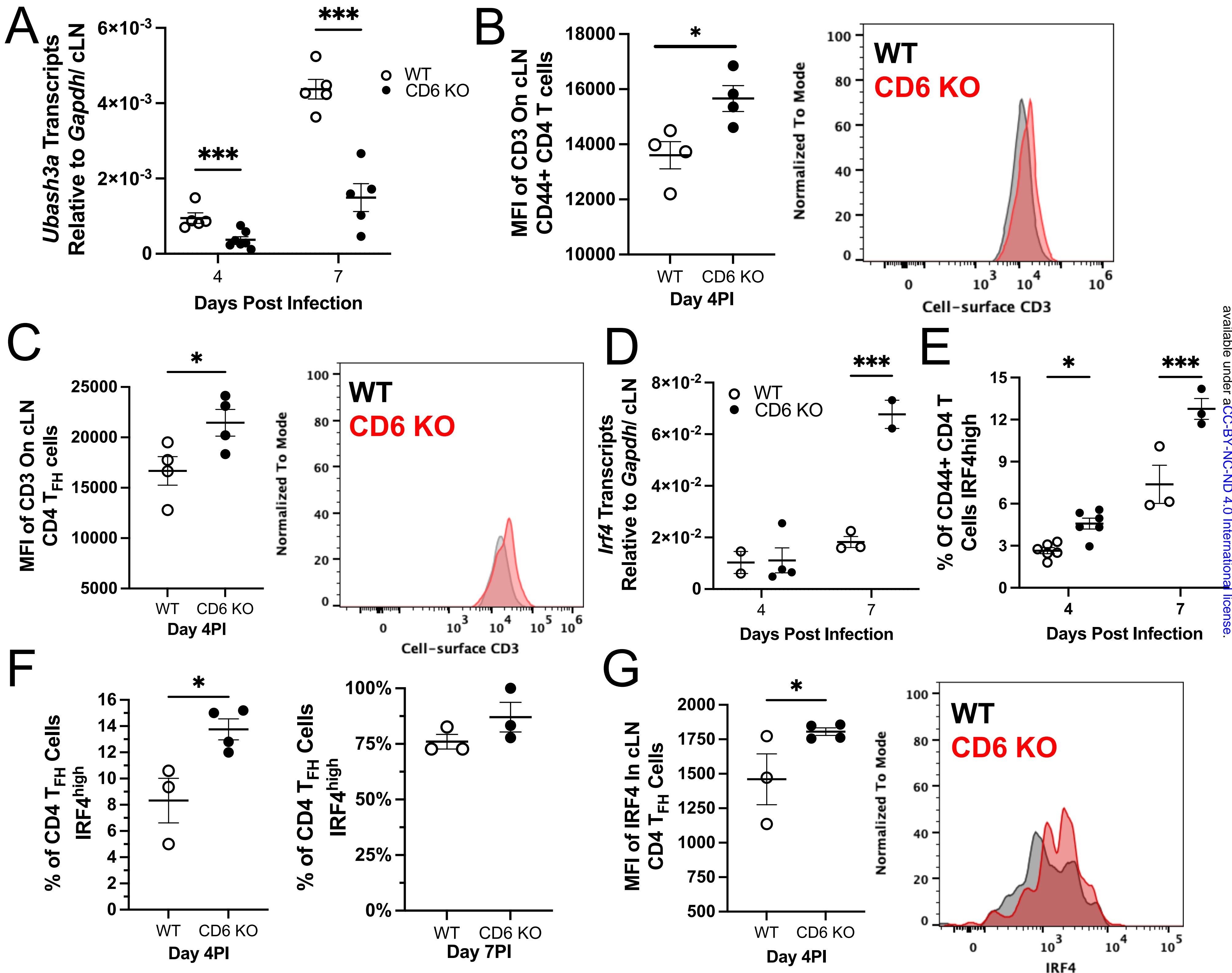

bioRxiv preprint doi: https://doi.org/10.1101/2024.07.26.605237; this version posted July 26, 2024. The copyright holder for this preprint (which was not certified by peer review) is the author/funder, who has granted bioRxiv a license to display the preprint in perpetuity. It is made available under aCC-BY-NC-ND 4.0 International license.